Characterization and Analyses on Complex Melting, Polymorphism, and Crystal Phases in Melt-Crystallized Poly(hexamethylene terephthalate)

Arup K. Ghosh, E. M. Woo,* Ya-Sen Sun,† Li-Ting Lee, and Ming-Chien Wu

Department of Chemical Engineering, National Cheng Kung University, Tainan, 701-01, Taiwan

Received December 21, 2004; Revised Manuscript Received April 11, 2005

ABSTRACT: Techniques of thermal analysis, wide-angle X-ray diffraction, and small-angle X-ray scattering were used to reveal relationships between complex melting behavior and various crystal forms in a polymorphic polymer. Correlation between the multiple melting endotherms and polymorphic crystalline forms in poly(hexamethylene terephthalate) (PHT) is a very intriguing one, which shows a maximum of six polymorphic melting endotherms (P_1-P_6) and up to two spherulitic forms packed with α- and β-crystal cells upon melt-crystallization at most temperatures. While the peaks P_1 and P_3 have been earlier assigned to the melting of the α-form and the peaks P_2 and P_5 are attributed to the β-forms, however, P_4 was yet to be resolved, which was absent in PHT melt-crystallized at lower temperatures. In this study, the fourth peak, P_4, was further resolved by high-temperature annealing of precrystallized PHT, and it was found to be associated with the most perfect and thus the thickest crystalline lamellae of α-forms. Correlation between the complex melting peaks and crystalline polymorphs in PHT was more successfully refined by employing combined techniques.

1. Introduction

Studies on the melting behaviors of semicrystalline polymers including syndiotactic polypropylene (sPP),[1,2] syndiotactic polystyrene (sPS),[3] poly(ether ether ketone) (PEEK),[4,5] poly(1,4-phenyl sulfide) (PPS),[6] and terephthalic polyesters like poly(ethylene terephthalate) (PET)[5,7,8] and poly(butylene terephthalate) (PBT)[9−12] have been vastly reported in the literature pertaining to polymer science. The complex multiple melting characteristic of these polymers, which is further complicated by the presence of polymorphic crystallites in some the polymers (e.g., sPS, sPP, etc.), evokes more challenge in discerning the origin of melting peaks. Two general mechanisms have been proposed in the literature to explain the multiple melting behavior, which may vary from a polymer to another polymer. First, the most widely discussed one is the heating scan-induced melting/recrystallization/remelting of the crystalline lamellae, which is mainly based on the behavior of endotherms obtained from the differential scanning calorimetry (DSC).[13,14] A reorganization model describes the transformation of less stable and/or imperfect flat-on lamellae to more stable/perfect edge-on lamellae through melting/recrystallization upon scanning to higher temperatures. The alternative proposition is based on the presumption of preexisting crystalline entities (dual/multiple), which includes the crystalline substructures like lamellae and spherulites present in the semicrystalline polymers.[4,15] Thus, it is imperative to interpret the multiple melting peaks in terms of the different crystalline forms present in the bulk of the polymer matrix.

Recently, the multiple melting behaviors of three homologous series of terephthalic polyesters, i.e., poly(trimethylene terephthalate) (PTT),[16] poly(pentamethylene terephthalate) (PPT),[17] and poly(hexamethylene terephthalate) (PHT),[17,18] have been reported. PTT crystallizes in triclinic structure like PET, but in the oriented fibers, only the fully extended form is observed for PET, whereas the contracted form is solely found in PTT. The multiple melting peaks in PET are attributed to the coexisting multiple crystalline entities with a broad distribution of lamellar thickness during normal scanning, and reorganization only occurs by extended annealing at specified temperatures.[7] However, for PTT, the multiple melting could very well be caused by either preexisting lamellae of different thickness or a consequence of the melting/reorganization process.[16] On the contrary, for both PBT[19] and PPT,[20,21] two distinct crystal forms were identified and defined in terms of α- and β-forms with triclinic chain packing. However, on mechanical deformation structural transformation from the α-form (contracted conformation) to the β-form (extended conformation) occurs in both polymers. The polymer chain of PPT on normal annealing crystallizes to the unique α-form, which remains intact with changing the crystallization temperature and/or thermal treatments.[17] Thus, the multiple melting behavior of annealed PPT can only be described in terms of melting/recrystallization model due to absence of any polymorphism. PHT yields three different types of crystalline structures depending on thermal and/or solution treatments, which are designates as α-, β-, and γ-forms.[22−24] The α-form in PHT with a monoclinic chain packing is favorably formed by crystallization under stressed condition. Both the β- and γ-forms of PHT are pertaining to same triclinic chain packing, and the former can be obtained by high-temperature annealing, while the latter is found in solvent-induced crystallization at room temperature. However, the γ-forms can be transformed into the other structures by annealing or orientation. Owing to the complexity in PHT crystal polymorphism, it may be instructive to readers to repeat and to summarize here the cell parameters of these three crystal forms in PHT, shown in Table 1 (data taken from a cited reference).[22] The melting behavior of PHT has not been explored extensively, and only a few reports

† National Synchrotron Radiation Research Center, 101 Hsin-Ann Road, Hsinchu Science Park, Hsinchu 30077, Taiwan.

* To whom correspondence should be addressed: E-mail: emwoo@mail.ncku.edu.tw.

10.1021/ma0473667 CCC: $30.25 © xxxx American Chemical Society
Published on Web 00/00/0000 PAGE EST: 10.6

Table 1. Crystal Cell Parameters[a] and Crystal Forms Showing the Polymorph in PHT[22]

crystal form designations	α	*β*	*γ*
crystal geometry	monoclinic	triclinic	triclinic
unit cell parameters			
a (nm)	0.91	0.48	0.53
b (nm)	1.72	0.57	1.39
c (nm)	1.55	1.57	1.55
α (deg)	127.3	104.4	123.6
β (deg)	90	116.0	129.6
γ (deg)	90	107.8	88.0
no. of chains/unit cell	6	1	2
unit cell density (g cm^{-3})	1.284	1.262	1.251
condition of formation	crystallization under stress (e.g., fiber drawing to high orientation)	annealing at high temp (∼140°C)	solvent-induced crystallization at room temp

[a] Note: parameters in this table are mainly taken from a cited reference,[22] reproduced here for helping clarity in discussions (upon suggestion during the refereeing process).

related to the multiple melting characteristics of oligomeric PHT and its copolymers with poly(ϵ-caprolactone) (PCL),[25] poly(hexamethylene 2,6-naphthalate) (PHN),[26] and isophthalic acid are available to date.[27,28] The complex melting peaks of PHT were broadly assigned either to different crystalline structures (crystal lattices or lamellae of different thickness) or to reorganization of these crystallites during melting. But, the correlation between the melting peaks and the individual unit-cell crystal forms (polymorphic) were not provided due to complicated melting patterns of PHT.

Only recently, the multiple melting behavior of thermally annealed PHT were reported in terms of two polymorphic crystalline forms α and *β*, and the origin of numerous endotherms was defined by two mechanistic approaches dual modification and reorganization.[18] The relationship among the crystal structure and spherulitic morphology in the melt-crystallized PHT was established. A maximum of five melting peaks (P_1-P_5) were obtained in DSC scanning of PHT melt-crystallized at low-to-medium temperature (90−130 °C), which gradually reduced to only a single melting peak when crystallization temperature was increased to 140 °C. Further analysis revealed that the α-form is the favored lattice (in a mixture of α- and *β*-forms) at medium crystallization temperatures and forms a Maltese-cross type spherulitic morphology. On the contrary, the sole *β*-form is the preferred lattice in PHT at high temperatures of crystallization, which packs into dendritic spherulites. During DSC scanning the α-form can be melted and recrystallized to thicker/perfect lamella or melted and transformed to the more stable *β*-form. However, the possibility of transformation of *β*- to α-form was nullified. In addition, it has been reported that the first two low-temperature endothermic peaks (P_1 and P_2) are due to the melting of originally existing PHT crystals with α-form packing, while the highest temperature endotherm (P_5) was believed to be associated with the dendritic spherulites consisting of sole *β*-forms of PHT. Moreover, incorporation of organically modified layered silicates into PHT matrix further resolved the melting peaks and led to more refined conclusion that endothermic peak P_2 is rather attributed to the thinner crystalline lamellae of *β*-forms and crystallites associated with P_3 is most likely due to the originally existing thicker lamellae of α-forms.[29] However, the origin of P_4 is rather more intriguing to explore, as it appears as a separate entity only at lower crystallization temperature along with other melting peaks. At such lower temperature, a dual crystalline morphology attributed to a mixture of both α- and *β*-forms of PHT prevails, which further complicates the analysis of P_4 endotherm. Thus, it is a challenging task to attempt clear and complete correlations between two polymorphic crystalline forms and numerous melting endotherms of PHT. Our objective was to further clarify the above issue and to identify the possible crystalline phase transformation due to thermal scanning and/or annealing by performing thorough and systematic studies on melt-crystallized PHT followed by logical analyses.

2. Experimental Section

2.1. Materials. PHT was synthesized using butyl titanate as catalyst according to the method reported earlier.[17,30] The weight-average molecular weight (M_w) and polydispersity index (PDI) measured by gel permeation chromatography (GPC) are 13 800 g/mol and 2.0, respectively. The apparent melting temperature of 144.5 °C for the synthesized PHT was characterized using a DSC, and $T_g = -6.7$ °C. Note that the polymeric chain in the synthesized PHT contains at least 30 repeat units. At this MW, maybe the mechanical properties are on lower sides, but its thermal and physical properties (T_g, T_m, crystallization, crystals, etc.) are expected to be closely characteristic of a polymer. Some of thermal transition temperatures in this PHT may be slightly lower than a really longer-chain PHT, but the characteristic of crystals, multiple melting peaks, remained almost the same as those in longer-chain PHT.

2.2. Characterization and Apparatus. 2.2.1. Differential Scanning Calorimetry. The melting behavior of the PHT samples was investigated using a differential scanning calorimeter (DSC-7, Perkin-Elmer) equipped with a mechanical intracooler under nitrogen purge to ensure minimal sample degradation. Temperature and heat flow calibrations at different heating rates were done using indium and zinc. Data were collected and peaks deconvolution was analyzed by using a Pyris software (Perkin-Elmer Corp.). For melt-crystallization treatments, samples were first melted at 180 °C for 10 min and quickly cooled (quenching) at a rate of −320 °C/min to desired isothermal temperatures (120−140 °C). Note here that −320 °C/min cooling rate can be set up but actually not fully realized because the actual cooling may be slightly lower than the set rate, owing to heat transfer hindrance. Even the actual cooling rate was less than the setup, the PHT samples were still effectively quenched into amorphous state. Another method of more effective quenching included melting, dipping the sample pans into a liquid N_2 container, and then placing into DSC cells. However, the problem of moisture sipping into DSC samples pans could be hard to deal with, and thus liquid N_2 dipping was not used unless there were no other alternatives.

For determining the transition temperatures, a dynamic heating rate of 10 °C/min was used unless otherwise indicated. Annealing treatment was performed for better resolution of the melting peaks. The samples were heated to the annealing temperature at a heating rate of 10 °C/min after melt crystallization at 130 °C for 120 min and annealed at the desired

temperature for further 120 min. The overlapped melting peaks were properly deconvoluted, and the DSC profile was separated into several components by the software Origin 6.1. Peak-fit routines were used to fit the thermogram to separate the different endothermic peaks associated with the various types of crystalline lamellae using Gaussian peak function. The Gaussian peak function is as follows:

$$f(x) = f_0 + \frac{H}{\sqrt{\pi/2}} e^{-2[(x-x_c)/w]^2} \quad (1)$$

In eq 1, x_c is the peak position, w is the full width at half-maximum, and H represents the height of the peaks. The programs were allowed to evaluate, by nonlinear curve fitting of experimental data, the height, the full width at half-maximum, and the position of individual components.

2.2.2. Wide-Angle X-ray Diffraction. Wide-angle X-ray diffraction (WAXD) was carried out on a Shimadzu XRD-6000 with Cu Kα radiation (30 kV and 40 mA) and a wavelength of 0.1542 nm. The scanning 2θ angle ranged between 2° and 30° with a step scanning rate of 2°/min. For direct comparisons, specimens of X-ray characterization were prepared using the similar thermal treatments as described for thermal analysis samples.

2.2.3. Optical Microscopy. A polarized-light microscopy (PLM, Nikon Optiphot-2) equipped with a camera, and a microscopic heating stage (Linkam THMS-600 with TP-92 temperature programmer) was used to investigate the spherulitic morphology of isothermally crystallized samples. The samples were pressed into a thin film between two glass slides by heating to melt on the hot stage at 180 °C for 10 min and then rapidly quenched down to the designated temperature (120−140 °C). The same temperature controlled heating stage was used for annealing of the PHT samples and were finally quenched to liquid nitrogen to freeze and terminate the process.

2.2.4. Small-Angle X-ray Scattering. We employed small-angle X-ray scattering (SAXS) to characterize the crystalline lamellar morphology of PHT subjected to the same thermal treatments as DSC thermal analysis samples. SAXS experiments were performed at BL01B SWLS beamline at the National Synchrotron Radiation Research Center, Taiwan. The incident X-ray beam was focused vertically by a mirror and monochromated to the energy of 10.5 keV by a silicon (111) double-crystal monochromator. The wavelength of the X-ray beam is $\lambda = 0.1181$ nm. The sample-to-detector distance is 1571 mm in length. The beam stop is a round molybdenum disk of 4 mm in diameter. With one-dimensional position-sensitive detector (PSD), we collected SAXS data. The sensitivity of PSD was calibrated by using a ^{55}Fe source before data collection. The calibration of the detector channels in terms of scattering vector was made by linear regression over the positions of numerous orders of the long spacing of silver behenate as the standard, with q_{max} being 1.076 nm^{-1}. The intensity profiles were output as the plot of scattering intensity (I) vs scattering vector, q ($q = (4\pi/\lambda)\sin(\theta/2)$, where θ is the scattering angle). The standard polyethylene (PE) sample was used to correct SAXS data so as to gain absolute intensity after background (air scattering) subtraction. All SAXS measurements were carried out at various temperatures in the hot stage under a dry nitrogen atmosphere. The specimens were in the sample cell sealed by two pieces of Kapton. Before measuring the SAXS profile at a given temperature, we waited for 0.5 min after attaining that temperature. Then the intensity distribution was accumulated for 2 min. The morphological parameters including long period (L), crystal lamellar thickness (l_c), and amorphous layer (l_a) were obtained from the one-dimensional correlation function according to standard procedures.[31]

2.2.5. SAXS Data Analysis. The normalized one-dimensional correlation function is defined as[31,32]

$$\frac{1}{\gamma(0)}\int_0^\infty I(q)q^2\cos(qz)\,dq \quad (2)$$

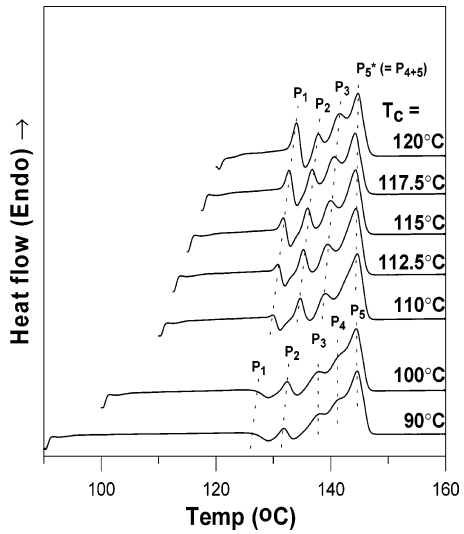

Figure 1. DSC thermograms (heating rate = 10 °C/min) of PHT melt-crystallized at different temperatures (90−120 °C) for 120 min (temperature of crystallization labeled on traces).

where z is the direction along which the electron density is measured. Q is just the scattering invariant:

$$Q = \frac{1}{2\pi^2}\int_0^\infty I(q)q^2\,dq \quad (3)$$

Since the experimentally accessible q range is finite, it is necessary to extend the SAXS data to both low and high q. Linear extrapolation to zero q is accomplished by the Debye−Bueche model

$$I(q) = \frac{A}{(1 + a_c^2 q^2)^2} \quad (4)$$

where A is a constant and a_c is the correlation length. A and a_c can be determined from the plot $I(q)^{-1/2}$ vs q^2 using the intensity data at the low q region (0.08−0.13 nm^{-1}). Extension to high q can be carried put using the Porod−Ruland (q^{-4} decay) model:

$$I(q) = K_p\frac{\exp(-\sigma^2 q^2)}{q^4} + I_{fl} \quad (5)$$

where K_p is the Porod constant and σ is a parameter related to the interface thickness between crystal and amorphous phases, and I_{fl} is the background intensity resulting from thermal density fluctuations. The values of K_p, σ, and I_{fl} were obtained by curve-fitting the intensity profile at the high q region (0.1−1.5 nm^{-1}).

3. Results and Discussion

3.1. Multiple Melting Behavior of Isothermally Crystallized PHT. Figure 1 exhibits DSC thermograms (10 °C/min) of the PHT samples isothermally melt-crystallized for 2 h at various temperatures (T_c) ranging from 90 to 120 °C (labeled on the individual traces). Numerous melting endotherms are apparent in all the DSC traces. As many as five distinct endotherms, labeled as P_1, P_2, P_3, P_4, and P_5 (from low to high temperature), are observed in PHT crystallized at 90 and 100 °C. The lamellar crystals associated with each of these five melting peaks are subsequently designated as P_1, P_2, P_3, P_4, and P_5 crystals. Moreover, two exotherms (crystallization peaks) are distinctly visible trailing the melting of P_1 and P_2. Both thermograms appear very similar, but P_2 increases in intensity with

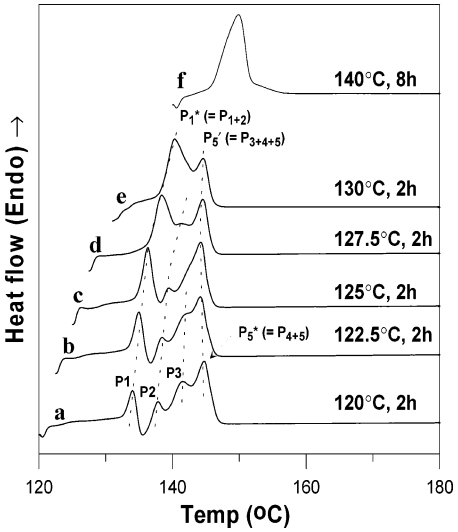

Figure 2. DSC thermograms (heating rate of 10 °C/min) of PHT melt-crystallized at different temperatures (120−140 °C, with temperature and time labeled a−f on the individual traces from bottom to top).

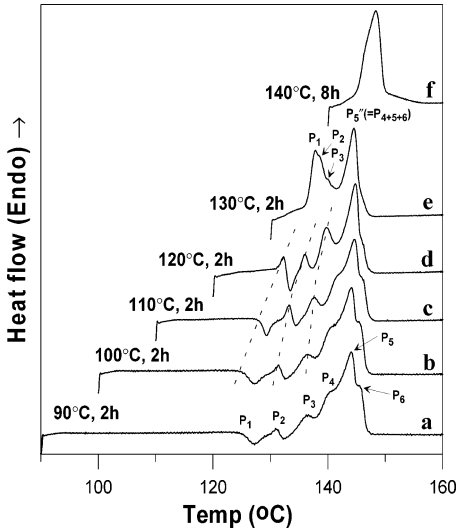

Figure 3. DSC thermograms (heating rate of 2.5 °C/min) of PHT melt-crystallized at different temperatures (120−140 °C, temperature and time labeled a−f from bottom to top traces).

the increase in T_c from 90 to 100 °C. Temperature positions of these melting peaks (except P_3 and P_5) also shift to higher temperature as the crystallization temperature is enhanced. Interestingly, only four endotherms can be observed during DSC scanning of PHT melt-crystallized at 110 °C (albeit sample crystallized for less than 60 min at the same temperature show five endotherms[18]). P_4 gradually shifts to a higher temperature with rise in crystallization temperature to 110 °C and eventually merges with P_5 to form one melting peak P_5^* (= P_{4+5}). Moreover, P_1 and P_2 become more apparent at this temperature, along with an exotherm in between them. On further increase in T_c to 120 °C, all the melting peaks shift to higher temperature. Samples were melt-crystallized at a temperature interval of 2.5 °C for better identification of the peaks. It is clear form this set of thermal scans that P_1 gradually emerges to be one of the most significant melting peaks with rise in crystallization temperature (along with P_5^*). P_2 remains almost constant in intensity, while that of P_3 increases considerably. However, both peak position (∼144.5 °C) and intensity of P_5^* remain almost unchanged throughout the range of crystallization temperature examined, which correspond to a nearly perfect and thermally stable crystalline lamellae. The presence of the recrystallization exothermic peak between P_1 and P_2 further indicates that the P_1 crystal developed at even 120 °C is not perfect enough to restrain melting/recrystallization during dynamic thermal scanning.

Figure 2 depicts the melting behavior of PHT crystallized at higher temperatures (120−140 °C), where the crystallization temperatures are labeled on the respective traces. A clear trend of peak shifting is observed with increase in T_c from 120 to 130 °C (through stepwise increment of 2.5 °C), and four endotherms at 120 °C gradually merge to exhibit only two melting peaks at 130 °C. P_1 increases significantly in intensity and gets broader with rise in temperature. The disappearance of recrystallization peak trailing P_1 at T_c = 125 °C further indicates the development of more perfect P_1 crystals at higher crystallization temperature. At T_c = 130 °C, P_1 becomes the most significant endotherm and P_2 seems to merge with P_1 to form a new peak P_1^* (= P_{1+2}). The highest melting peak (P_5^*) remains unchanged throughout the temperature range (120−130 °C). However, P_3 merges with P_5 at $T_c \sim 125$ °C to develop again a new peak P_5' (= P_{3+4+5}). Nevertheless, all the melting peaks eventually merge to a single peak in PHT samples melt-crystallized at an extremely high temperature of 140 °C (for 8 h).[18] The increase in the peak temperature to ∼150 °C also indicates the formation of thicker lamella consisting of a unique and more perfect crystalline form at T_c = 140 °C.

In DSC thermograms, a single melting peak may form due to superposition of several melting peaks or actual melting of only a single type of lamella. The melting endotherms were further resolved by slower heating rate, which sheds light on discerning the overlapped peaks. Figure 3 illustrates the melting pattern of PHT crystallized at different T_c (90−130 °C), at a scanning rate of 2.5 °C/min (the temperature and time of crystallization are labeled on the individual traces). The insignificant change in the relative contribution of the peaks and slight shifting in peak temperature with a decrease in heating rate (subsequent increase in resolution) indicate the presence of different crystalline structures (different crystal lattices or different lamellar thickness) rather than simple melting/reorganization of the imperfect lamella. Surprisingly, one more endothermic peak emerges (six peaks in total) in all the DSC traces of PHT samples crystallized up to 120 °C. The new peak is distinctly visible at highest temperature position trailing P_5, which is designated as P_6. The appearance of P_6 is attributed to the thickest crystalline lamellae (with highest thermal stability) formed by the melting/reorganization of initial crystals upon dynamic DSC scanning or due to preexisting crystal forms that have been developed during the original isothermal crystallization imposed on PHT. However, P_6 is no longer visible in the PHT samples crystallized at a temperature higher than 120 °C (at T_c = 130 and 140 °C), which is likely to be overlapped by very strong P_5 to develop a new peak $P_5'' = (P_{4+5+6})$ (P_4 already merges with P_5 at T_c = 120 °C). Interestingly, all the endothermic peaks P_1, P_2, and P_3 are evident (partially merged) along with P_5'' in the DSC trace of PHT crystallized at 130 °C, which further indicates at least existence of discrete and different lamellar types at such high temperature of crystallization. In accordance with ear-

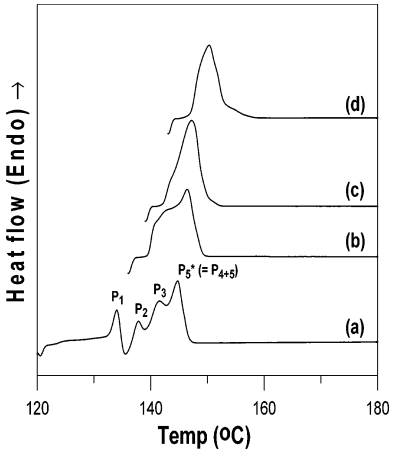

Figure 4. DSC thermograms (heating rate = 10 °C/min) of PHT melt-crystallized at 120 °C for 2 h: (a) as-prepared, (b) annealing at 136 °C for 2 h, (c) annealing at 139 °C for 4 h, and (d) annealing at 143 °C for 6 h.

lier reports, only a single endothermic peak of PHT is revealed at T_c = 140 °C for 8 h even by the DSC scanning rate of 2.5 °C/min, suggesting the melting of only one homogeneous crystalline lamellae.[18]

3.2. Crystalline forms of PHT melt-crystallized at 120 °C. It was reported earlier that the endothermic peaks P_1 and P_3 are due to the melting of α-form, while P_2 and P_5 were believed to be associated with the β-forms of PHT.[18,29] For further clarification of the crystalline forms attributed to the multiple melting endotherms of PHT, experiments were performed with DSC to impose various thermal events on the samples, which were identically melt-crystallized at 120 °C for 2 h to develop maximum crystallinity. Figure 4 exhibits DSC thermograms of PHT samples subjected to four different thermal treatments. The first sample was normally scanned at 10 °C/min from 120 to 180 °C just after the completion of crystallization, resulting in the total sum of melting enthalpy of P_1, P_2, P_3, and P_5* to 50.4 J/g (Figure 4a). The second sample was scanned from 120 to 136 °C at a rate of 10 °C/min and annealed at 136 °C for 2 h to complete the melting of P_1 and recrystallization. It was then scanned up at 10 °C/min from 136 to 180 °C, and a typical broad endotherm of several combined peaks was obtained (Figure 4b). The overlapped melting peaks were further decomposed to numerous component peaks (Figure 5) by using a peak-fitting software. Deconvolution of the merged endotherm of the second sample resulted in separation of the profile into several component peaks and revealed three melting peaks P_2, P_3, and P_5* (Figure 5a) with a total enthalpy for melting being 53.5 J/g. Similar number of endothermic peaks was also evident on slower thermal scanning (DSC thermograms are not shown here for brevity). The increment of total enthalpy by 3.1 J/g and shifting of peak temperatures of P_2, P_3, and P_5* to higher temperatures further indicates that once P_1 (thinner lamellae of α-forms) melted away in scanning, it fast rearranged into crystallites of higher melting temperatures like P_3 (α-forms having thicker lamellar structure) and/or P_4. The third samples was scanned from 120 to 139 °C at a rate of 10 °C/min and annealed at 139 °C for 4 h for completion of the melting of P_1 and P_2 and recrystallization of the same. It was further scanned up from 139 to 180 °C at a scanning rate of 10 °C/min and again a broad endotherm of multiple overlapped peaks resulted (Figure 4c). However, peak deconvolution revealed the individual P_3 and P_5* (Figure 5b) and the total enthalpy of melting is found to be 50.9 J/g. Nevertheless, P_3 was exhibited as only a shoulder to P_5 on slower DSC scanning (DSC thermograms are not shown here for brevity). The lowering of enthalpy suggests that melting of P_2 (thinner lamellae of β-forms) was not readily followed by repacking into P_4, P_5 (thicker lamellae of β-forms), and/or P_6. However, shifting of peak temperatures of P_3 and P_5* to higher temperatures suggests the development of more perfect crystals due to annealing at high temperature. The final samples was scanned from 120 to 143 °C at a rate of 10 °C/min and annealed at 143 °C for 6 h to melt P_1, P_2, and P_3, and recrystallization. It was then scanned up from 143 to 180 °C at a scanning rate of 10 °C/min to obtain a single and broad endothermic peak (Figure 4d). The total enthalpy of melting is 41.9 J/g and peak deconvolution yields two major (P_4 and P_5) and one minor endothermic peak (most likely of P_6) (Figure 5c). The existence of the numerous peaks was further verified by resolving the endotherm with slower scanning rate (2.5 °C/min), which yielded separate melting peak P_4 in the final sample. In other words, the identity of P_4 is still maintained after annealing at 143 °C for 6 h (DSC traces are not shown here for brevity). The lowering of enthalpy in fourth sample could imply that

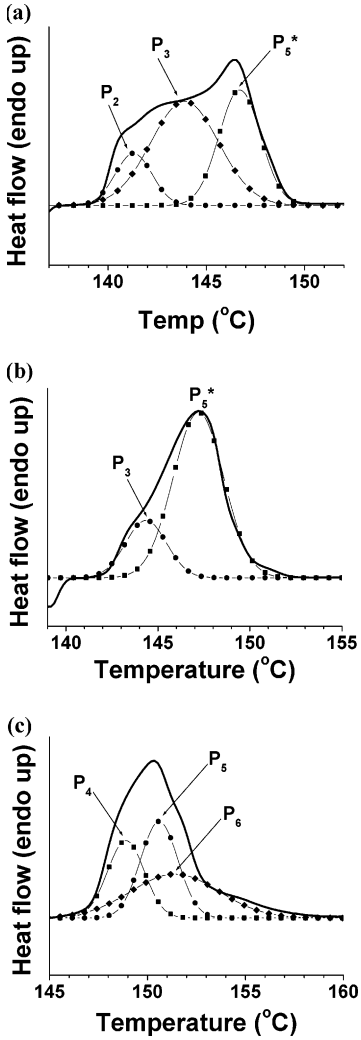

Figure 5. Deconvoluted DSC profiles (heating rate = 10 °C/min) of PHT melt-crystallized at 120 °C for 2 h and then further annealing at (a) 136 °C for 2 h, (b) 139 °C for 4 h, and (c) 143 °C for 6 h.

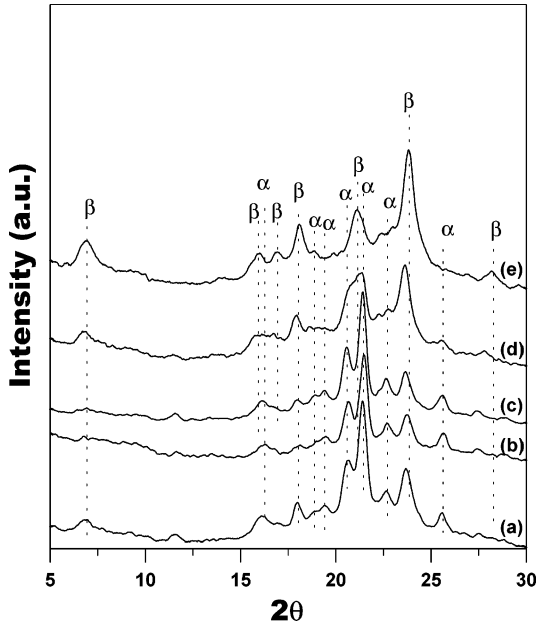

Figure 6. WAXD profiles of PHT melt-crystallized at 120 °C for 2 h: (a) as-prepared, (b) then further annealing at 136 °C for 2 h, (c) annealing at 139 °C for 4 h, (d) annealing at 143 °C for 6 h, and (e) melt-crystallized at 140 °C for 8 h.

P_3, which is associated with α-forms with thicker lamellae, cannot rearrange into other higher melting peaks (P_4, P_5, and P_6) readily even on annealing for long time at 143 °C. Nevertheless, the peak positions of P_4 and P_5 shifted to higher temperature, which indicates thickening of the crystalline lamella due to annealing.

It was already reported that the endothermic peak P_5 is attributed to the β-forms of PHT[18] and the highest melting peak P_6 is also most likely due to β-forms as α-forms cannot form at such high temperature. To shed more light on the crystalline forms that developed due to different thermal treatments, WAXD measurements of the annealed samples were carried out. Figure 6 presents WAXD patterns of these four samples similarly annealed as described above. The sample melt-crystallized at 120 °C (Figure 6a) exhibits the reflection of different types of crystalline forms: (i) α-form (monoclinic unit cell, $2\theta = 15.9$, 20.5, 21.2, and 25.4°) and (ii) β-form (triclinic unit cell, $2\theta = 7.2$, 17.9, and 23.6°). The diffraction pattern of PHT sample melt-crystallized at 140 °C (8 h) is also shown for better comparison (Figure 6e), and by a distinct contrast the peaks are observed at $2\theta = 7.2$, 15.8, 16.7, 17.9, 18.7, 21.0, 23.6, and 27.9°, which are due to the sole type of β-forms with no significant characteristic reflections for the α-form. The second (annealed at 136 °C for 2 h) and third samples (annealed at 139 °C for 4 h) exhibit almost similar diffraction patterns as the first sample (Figure 6b,c), which reveals the presence of both α- and β-forms. Moreover, comparing the intensities of two most significant peaks of the α-crystal at $2\theta = 20.5$ and 21.2°, one can qualitatively estimate slightly higher fraction of α-form in third sample as compared to the second one (considering equal weight and dimension of the samples). In contrast, the fourth sample (annealed at 143 °C for 6 h) shows a different WAXD trace (Figure 6d), where the significant peaks of β-forms ($2\theta = 17.9$ and 23.6°) are more apparent. However, the α-form is still present ($2\theta = 20.5$, 21.2, and 25.4°) in the sample, and the characteristic reflections of α-form at $2\theta = 20.5$ and 21.2° are likely to produce a broad peak due to the overlapping of a significant reflection of β-form at $2\theta = 21.0°$, which is distinctly apparent in the WAXD pattern of PHT sample melt-crystallized at 140 °C (Figure 6e). The existence of α-form in the fourth sample lends support in its attribution to the endothermic peak P_4, as this sample exhibits only three peaks (P_4, P_5, and P_6) (Figure 5c) (DSC thermogram at slower scanning rate also revealed separate P_4), of which the higher melting P_5 and P_6 are most likely due to the β-form of PHT (as described earlier). Furthermore, the population of α-phase in third sample was found to be slightly higher as compared to the second sample (Figure 6b,c), while the peak area of P_3 (α-form) showed a reverse trend (Figure 5a,b). Thus, from above observation, the increase of α-form in third sample can be justified by assigning it to the endotherm P_4 (here merged with P_5 and P_6 to form P_5*), which is likely to form due to the more perfect and thickest crystalline lamellae of α-form, on annealing at 139 °C for 4 h. However, on further annealing at 143 °C for 6 h (fourth sample), which is too close to the original melting peak of P_4 (∼144 °C in third sample, Figure 5b), a part of the α-form melted and may be repacked to β-form that can enhance the WAXD reflections of β-form in expense of the α-form.

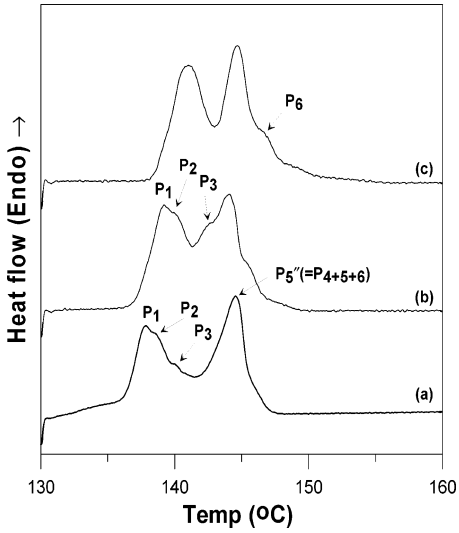

Figure 7. DSC thermograms of PHT melt crystallized at 130 °C for (a) 2, (b) 8, and (c) 24 h (heating rate = 2.5 °C/min).

3.3. Transition of Crystalline Phases in PHT. DSC thermogram of the PHT sample melt-crystallized at 130 °C for 2 h yielded only two endotherms (P_1* = P_{1+2} and $P_5' = P_{3+4+5}$) when dynamically scanned at 10 °C/min (earlier in Figure 2e). Interestingly, on further resolution of the melting peaks by slower scanning rate (2.5 °C/min) four peaks (P_1, P_2, P_3, and $P_5'' = P_{4+5+6}$) were revealed (Figure 3e). Thus, a significant change in peak formation and their temperature position is observed with decrease in DSC scanning rate. Further experiments were performed for detailed understanding of the effect of crystallization time (t_c) on the melting behavior and identification of the crystalline form associated with the resulting endotherms of PHT crystallized at 130 °C.

The complex melting behavior of PHT subjected to melt-crystallization at 130 °C for various times (2−24 h) is illustrated in Figure 7. P_1, P_2, and P_3 (having different lamellar structures) are visible as partially overlapped peaks, and P_5'' (= P_{4+5+6}) is apparent as a separate peak in the DSC trace (scanning rate = 2.5 °C/min) of PHT crystallized at 130 °C for 2 h (Figure

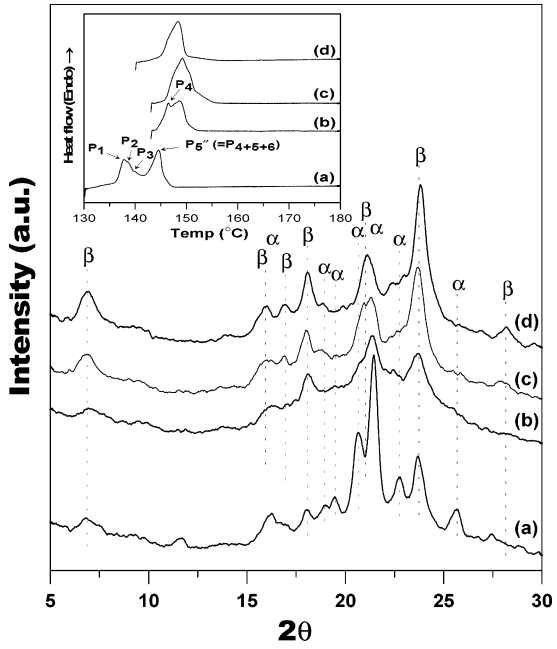

Figure 8. WAXD profiles of PHT melt crystallized at 130 °C for 2 h: (a) as-prepared, (b) after annealing at 143 °C for 2 h, (c) after annealing at 143 °C for 6 h, and (d) PHT melt-crystallized at 140 °C for 8 h (all samples scanned at 2.5 °C/min). DSC thermograms of the respective samples are shown inset.

7a). Temperature positions of P_1, P_2, and P_3 are enhanced with increase in t_c to 8 h (Figure 7b). The most significant increment in temperature is observed for P_3 (∼2.5 °C), but the peak temperature of P_5* remains almost constant (∼144.5 °C) while P_6 appears (∼145.5 °C) as a shoulder to P_5*. P_1 and P_2 eventually merge to develop a single peak at higher temperatures when t_c is increased to 24 h (Figure 7c). Moreover, P_3 also merges with P_5* to yield a stronger peak without changing the temperature position of P_5*, and P_6 is also distinctly apparent at a little bit higher temperature (∼146.5 °C). Thus, with increase in t_c the peak temperature of P_3 is most significantly shifted to higher value, while P_4 is never divulged as a separate peak. Again, at $t_c = 24$ h, P_3 merges with P_5* to produce a quite sharp peak, where P_3 and P_4 become indistinguishable. Thus, the thickness of crystalline lamellae of P_3 is likely to increase with annealing time and eventually become similar to that of the preexisting P_4 crystalline lamellae, which can be conceived as most perfect α-crystals that remains unchanged like P_5 (both merge to P_5*) with increase in t_c. However, P_6 is assumed to correlate the thickest lamellae of β-forms, which melts at significantly higher temperature (thermally more stable) than the α-forms. Its thickness continues to increase with t_c and results in higher peak temperature.

The crystalline form associated with the melting peak P_4 in PHT samples crystallized at 130 °C were elaborately analyzed by performing the thermal annealing treatments. Figure 8 depicts WAXD patterns of PHT samples subjected to three different thermal events. DSC thermograms (scanned up to180 °C at a heating rate of 2.5 °C/min) of the same samples are shown inset. The diffraction pattern and DSC trace of PHT sample melt-crystallized at 140 °C are also shown for better clarification of the crystalline forms (Figure 8d). First one is the typical PHT sample melt-crystallized at 130 °C for 2 h (total enthalpy of melting is 55.4 J/g), which shows a combination of α- and β-crystalline forms pertaining to the endotherms P_1, P_2, P_3 (merged), and P_5'' (= P_{4+5+6}) (Figure 8a). The second sample was scanned from 130 to 143 °C at a rate of 10 °C/min after melt-crystallization at 130 °C for 2 h and annealed at 143 °C for 2 h to complete the melting of P_1, P_2, and P_3 and recrystallization. The treated sample (Figure 8b) yields a characteristic broad peak in WAXD pattern at $2\theta \sim 20-22°$ due to the overlapped reflections of α-form ($2\theta = 20.5$ and 21.2°) and β-form ($2\theta = 21.0°$, which is prominent in the WAXD trace of melt-crystallized PHT at 140 °C (Figure 8d)). In DSC thermogram, the tip of the P_4 endotherm is apparent (at higher temperature position) (inset, Figure 8b) similar to the sample crystallized at 120 °C and scanned at a heating rate of 2.5 °C/min, which signifies coarsening of crystalline lamellae that are different from P_5 and P_6. However, the weak intensity of characteristic reflections of β-form at $2\theta =$ 7.2, 17.9, and 23.6° further indicates a lower degree of crystallinity in the sample, and total melting enthalpy of 32.5 J/g indicates very less recrystallization of P_1, P_2, and P_3 may be due to insufficient annealing time. To enhance the crystallinity, the third sample was melt-crystallized at 130 °C for 2 h, then scanned from 130 to 143 °C at a rate of 10 °C/min, and annealed at 143 °C for 6 h. Evidently, the diffraction peaks of β-forms (2θ = 7.2, 17.9, 21.0, and 23.6°) are increased significantly in intensity (Figure 8c), while the characteristic reflections of α-form ($2\theta = 15.9$ and 21.2°) are still apparent (almost unchanged) in the WAXD pattern. However, the melting peak P_4 is absent in the DSC thermogram (inset, Figure 8c), which is shifted to higher temperature and seems to merge with P_5 to develop a broader endotherm of significantly high melting enthalpy (49.5 J/g). Almost identical merging of P_4 and P_5 was observed in the case of PHT melt-crystallized at 120 °C (heating rate = 2.5 °C) and then annealed at 143 °C for 12 h, but they remained separate when annealed up to 6 h (DSC traces are not shown here for brevity). This observation is justified by the fact that P_4 is associated with more perfect crystalline structures when PHT is melt-crystallized at 130 °C than that crystallized at 120 °C. Hence, the melting temperature of P_4 is higher in the former sample (crystallized at 130 °C), which is nearer to that of P_5. Since the peak temperature of P_5 almost remains constant, P_4 merges with P_5 within a shorter annealing time (6 h), but for the latter sample (crystallized at 120 °C) it takes almost 12 h of annealing time for occurrence of merge of P_4 and P_5. The peak position P_4 and P_5 (merged) is further shifted to higher temperature (which is even higher than that of PHT sample crystallized at 140 °C for 8 h (inset, Figure 8c)), and P_6 is apparent only as a shoulder. Higher annealing time leads to better reorganization of initial crystals P_1, P_2, and P_3 (through melting upon DSC scanning) and also thickening of preexisting crystalline lamellae (P_4, P_5, and P_6). Nevertheless, the population of β-form is enhanced with increase in annealing time at 143 °C and becomes dominant after 6 h of annealing, as the formation of α-form reduces with increase in temperature.[18] Thus, the endothermic peak P_4, which forms likely due to the melting of α-forms, eventually becomes insignificant (merges with P_5) as compared to P_5 and P_6 (consisting of β-forms) on annealing at considerably high temperature near to its melting temperature.

Additionally, the dual spherulitic morphologies of PHT samples subjected to melt-crystallization at 130 °C and

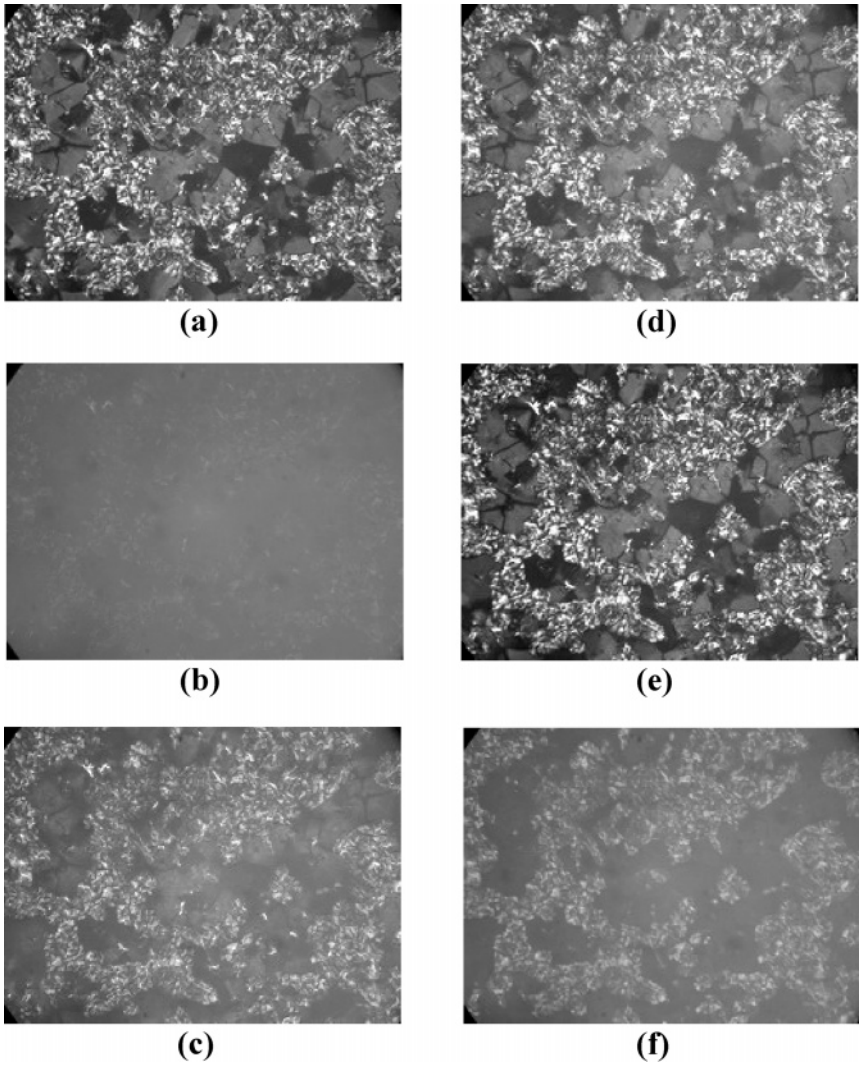

Figure 9. PLM micrographs of PHT melt-crystallized at 130 °C for 2 h: (a) as-prepared, (b) after annealing at 143 °C for 1 min, (c) after annealing at 143 °C for 5 min, (d) after annealing at 143 °C for 2 h, (e) after annealing at 143 °C for 6 h, and (f) further heating to 148 °C (heating rate = 10 °C/min).

higher temperature annealing were studied by optical microscopy. Generally, at higher crystallization temperature (T_c > 120 °C), the PHT crystalline lamella assumes two different types of spherulite with significantly large dimension, one being a typical Maltese-cross type and the other resembles a dendritic spherulite. It has been also reported that the lower melting Maltese-cross spherulite consists of α-forms; on the contrary, the higher-melting β-forms are packed to a dendritic spherulite. However, the PHT sample crystallized at 140 °C exhibits a unique dendritic spherulite containing entirely β-form.[18]

Figure 9 shows optical micrographs of PHT sample at different time interval while annealing at 143 °C after melt-crystallization at 130 °C for 2 h and scanned up to 143 °C at a rate of 10 °C/min. A dual crystalline morphology (Maltese-cross and dendritic-type spherulites) is evident in the sample melt-crystallized at 130 °C for 2 h (Figure 9a). As the sample was heated to 143 °C (to melt P_1, P_2, and P_3), a hazy and smoky picture resulted at the first minute, which is possibly due to partial melting of the crystalline species (as the dendritic species are still apparent) (Figure 9b). However, within 5 min the crystalline morphology reappeared and dendritic spherulites are distinctly apparent, while the Maltese-cross spherulites are still almost dark as amorphous phase (Figure 9c). After 2 h of annealing (Figure 9d) almost all the Maltese-cross spherulites are apparent along with the dendritic ones, and the morphological pattern looks very similar to the first sample (Figure 9a). Moreover, the micrograph looks very clear on annealing the sample for 6 h (Figure 9e), and an unaltered crystalline pattern is evident. Nevertheless, on further heating of the sample to 148 °C (for melting P_4) a preferential melting of the Maltese-cross spherulites was observed to yield dark amorphous phase admixed with intact dendritic type spherulites (Figure 9f), which eventually melted at higher temperature.

The above observation further lends support in the correlation between α-forms and melting peak P_4. The Maltese-cross type spherulites present even after annealing at 143 °C are most likely to contain the thickest crystalline lamellae of α-forms and are manifested as the P_4 endotherm with a lower melting temperature than P_5, as they evidently melt before the dendritic spherulites (β-forms) on heating beyond 143 °C. Moreover, an additional point has been surfaced from the PLM observation, which is imperative to be addressed for further clarification of the transformations of PHT crystalline phases. The PLM micrographs of PHT sample crystallized at 130 °C and annealed at 143 °C for 2 and 6 h (Figure 9, d and e, respectively) depict

almost identical morphological pattern as that of the as-prepared (not-annealed) sample (Figure 9a). It was earlier discussed that the Maltese-cross spherulites are of the α-form, while the crystalline lamellae containing β-form generates dendritic spherulites.[18] Nevertheless, the WAXD profiles of the samples subjected to similar thermal treatments revealed significantly different pictures. PHT sample crystallized at 130 °C evidently contains a predominant fraction of α-forms admixed with β-forms (Figure 8a), while in the annealed (at 143 °C) samples the population of β-form is increased with annealing time and after 6 h of annealing β-forms are found in major proportion (Figure 8c). Thus, it is difficult to correlate the crystalline forms of PHT with the evolved phase morphology by imposing thermal annealing treatments, as after annealing the fraction of β-form is significantly enhanced, which is not reflected in its spherulitic morphology. A probable reasoning can be provided to explain this phenomenon. On dynamic heating from 130 to 143 °C the thinner lamellae of α-form (pertaining to P_1 and P_3) of PHT melted and likely reorganized either to more perfect and thicker crystalline lamellae of P_4 which has similar spherulitic morphology (Maltese-cross type) or partially to P_5 (and/or P_6) attributing dendritic spherulites (β-form). But the rate of formation of α-forms is reduced with increase in temperature, so the recrystallization of P_1 and P_3 to α-form becomes less probable at such high temperature of annealing. This can further be supported by the fact that PHT on cold-crystallization at 140 °C yields only the dendritic spherulites pertaining to sole β-forms;[17] i.e., at high temperature ($T_c \geq 140$ °C) no α-forms are developed and only β-form prevails. Thus, presence of the α-form in PHT at 143 °C is more likely due the preexisting α-forms of higher melting temperature (i.e., P_4). However, at such high temperature of annealing at 143 °C which is very near to the peak temperature of P_4, there was a strong possibility that at least a part of the lamellar structure of P_4 could melt and remained as amorphous at the interlamellar zone. Thus, overall Maltese-cross-type morphology remained intact, but the crystallinity of the α-form was lowered, which is reflected in WAXD profiles. Nevertheless, the crystalline lamella contributing to the β-form continued to become more perfect and thicker to form P_5 and P_6, which could further be facilitated by the melting/reorganization of P_1, P_2, P_3, and even P_4 (partial) and resulted in enhanced intensity of diffraction peaks corresponding to the β-forms.

The double melting at 130 °C may be due to the consequence of sequential melting of thinner lamellae ($P_1 + P_2 + P_3$) and thicker lamellae combined ($P_4 + P_5$) with recrystallized crystallites with good lateral crystal perfection (P_6). To examine this hypothesis, we employed in-situ SAXS measurements on PHT in the course of heating/annealing. Figure 10 reveals the profiles of SAXS intensity (I) of semicrystalline PHT melt-crystallized at 130 °C (120 min) and then postannealed at 143 °C for various time. For PHT melt-crystallized at 130 °C, the SAXS clearly shows strong lamellar scattering. The long spacing (L) can be evaluated as 18.3 nm from Bragg's law ($L = 2\pi/q$). Upon raising temperature to 143 °C, the peak depresses significantly and its position shifts toward lower angles immediately at the beginning. It becomes evident with increasing annealing time. This evidence provides that the thinner crystal lamellae melt, then form amorphous

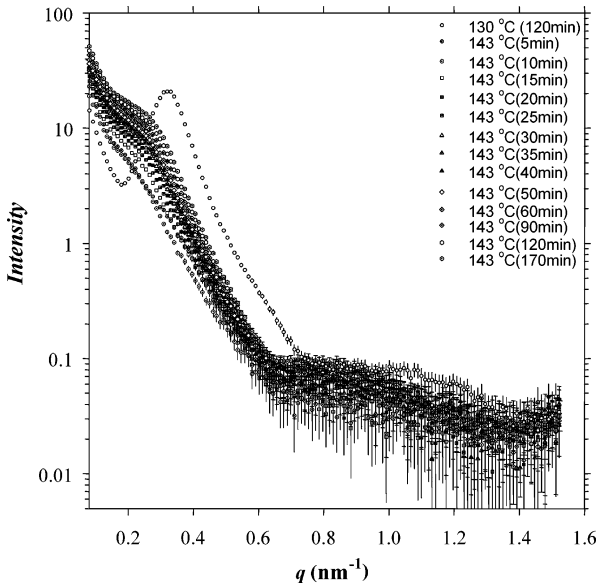

Figure 10. SAXS profiles of PHT melt-crystallized at 130 °C for 2 h and subsequently postannealed at 143 °C for various time. The given times are indicated in the figure.

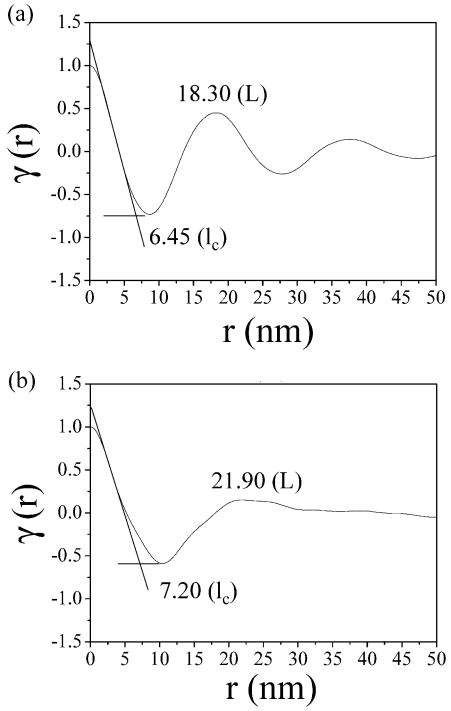

Figure 11. One-dimensional correlation functions and associated parameters for PHT: (a) melt-crystallized at 130 °C for 120 min and (b) then postannealed at 143 °C for 170 min.

phase, and finally recrystallize into thicker crystal lamellae with high thermal stability at low recrystallization rate. Thus, a possibility of crystal-to-crystal transition prior to melting of thinner crystal lamellae can be ignored. In the lamellar stack mode,[31,32] the long period represents the sum of the crystal lamellar thickness (l_c) and amorphous layer (l_a). Rise in the long period may thus result from the thickening of crystals or swelling of amorphous layers due to thinner crystal lamellar melting upon heating. The morphological feature is further revealed by one-dimensional correlation function of SAXS curves of PHT under melting condition, as shown in Figure 11. Determination of long period (L) may be realized by locating the first maxi-

mum in the one-dimensional correlation function. The first minimum may be either l_c or l_a depending on the linear crystallinity (ϕ_C^{lin}) of PHT. Linear crystallinity is defined as[33,34]

$$\phi_C^{lin} = \frac{l_c}{L} = \frac{l_c}{l_c + l_a} \quad (6)$$

By considering that spherulites are volume filling, ϕ_C^{lin} is related to the bulk crystallinity, ϕ_C, measured by thermal analysis. According to a value of 144 J/g for 100% crystalline PHT proposed by David et al.,[28] it is reasonable to assign the first minimum as l_c when the linear crystalline is smaller than 0.5 (a value of ϕ_C = 0.385 for PHT melt-crystallized at 130 °C for 120 h by DSC). L, l_c, and l_a are 18.3, 6.45, and 11.85 nm, respectively, for 130 °C crystallized PHT. When this sample was postannealed at 143 °C for 170 min, the average lamellar thickness increased as indicated by l_c = 7.2 nm, and also a corresponding long period increased to L = 21.9 nm. A large increase in amorphous thickness ($l_a = L - l_c$) by 2.85 nm may be due to partial melting of the thinner crystalline between the existing thicker lamellar stacks. By contrast, the average crystal crystalline lamellae seem to increase slightly. Apparently, as the heating temperature is increased to ~7 °C below the final melting temperature, there is still some recrystallization. However, such a recrystallization proceeds extremely slowly due to confined space imposed by the remaining thicker primary lamellar stacks. Finally, the most amorphous phase may have been trapped between these stacks, giving rise to the large increase observed in the long period.

From the SAXS and WAXD results, we found that reorganization of lamella occurred in the length scale ranging from unit cell on the molecular scale-up to crystal lamellar crystalline of the size on the order of nanometer. Owing to the confined space provided by the unmelted primary lamellae, the amorphous polymer chains deriving from melting of thinner lamellae (P_1 + P_2 + P_3) between these lamellae (P_4 + P_5) may be unable to diffuse to the regions between spherulites (i.e., interspherulite). This decreases the possibility of having interspherulitic crystallization in which the growth front can advance to generate the spherulites with large size. Under these circumstances, however, there is the possibility of generating interlamellar crystallization where the thicker lamellae due to recrystallization may form in the existing thicker lamellae (P_4 + P_5). SAXS results further confirm PLM studies of PHT, indicating that the reorganization upon heating does not involve changes in the spherulitic pattern or sizes.

General Discussions on Melting Peaks and Polymorphism in PHT. Apparently, the five melting peaks (P_1−P_5) seen in the low-T melt-crystallized PHT are not all associated with a single-crystal cell, but rather with two different crystal cells (α and β). At higher crystallization temperatures (140 °C and up), however, only the β-crystal cell is present in PHT, which exhibits a decreasing number of melting peaks. The fraction of β-form in PHT increases significantly at expense of the α-form through melting/recrystallization, though no evidence of solid−solid transformation is seen. A portion of the crystalline lamellae (α-form) may melt into amorphous constituents at the interlamellar zone to be followed by recrystallization into thicker lamellae consisted of β-form crystal, which reduces the fraction of α-form while maintaining the overall Maltese-cross-type morphology intact. However, a significant depression in the recrystallization process in terms of lamellar thickening at a higher temperature of 143 °C consequently promoted the extent of the amorphous regions between the existing thicker lamella. Subsequent growth of the lamellae between these regions underwent gradually a great deal of crystal perfection with time. Therefore, clarification can be made on the great number of melting peaks seen in low-T melt-crystallized PHT that originally contains two crystal cells. But annealing (or heat-scanning) at higher temperatures tends to uniformize the lamellar sizes, and the original polymorphic crystal cells are reorganized into a single one (β-form). In addition, it should be interesting to explain the spherulitic morphology seen in PHT in comparison to other aryl polyesters, such as poly(trimethylene terephthalate) (PTT) and poly(pentamethylene terephthalate) (PPT). Both PTT and PPT exhibit ringed patterns in spherulites within a temperature window of crystallization. But PHT exhibits no ring patterns (Figure 9) at all temperatures, which is similar to poly(butylenes terephthalate) (PBT). Interestingly, the number of methylene groups between the terephthalate groups seems to determine the lamellar orientation within the spherulite. This is true for homologous series of aryl polyesters but may not be so for other types of polymers.

4. Conclusions

PHT was found to exhibit a maximum of six melting endotherms (P_1−P_6) that are pertaining to two crystalline polymorphs (α and β). Except for P_5 and P_6, which are associated with thicker crystalline lamella of β-form, all the lower-melting peaks gradually can shift to a higher temperature with increase in the crystallization temperature from 90 to 130 °C. Upon annealing at T_c = 130 °C, PHT exhibited only two melting endotherms. However, the lower melting peaks were further revealed on DSC scanning at slower rates, presence of different crystalline structures. All the peaks were found to eventually merge with P_5 to yield a unique melting peak at T_c = 140 °C, indicating a homogeneous crystalline lamellae. While the crystalline lamellae associated with P_1 and P_3 were reported to be of the α-form and those of P_2 and P_5 were attributed to the β-form, the nature of crystalline structure related to P_4 could not be distinguished as P_4 tends to merge with P_5 at an even lower T_c of 110 °C to form one high-temperature melting peak. However, in this study P_4 was discernible as a separate entity in the precrystallized (at 120 and 130 °C) PHT after annealing at higher temperature.

WAXD and SAXS analyses of these thermally annealed samples further revealed most likely association of the endothermic peak P_4 with melting of the perfect and thickest crystalline lamellae packed by the α-forms of PHT. Moreover, the gradual merging of P_3 with P_4 with increase in crystallization time in the PHT sample crystallized at 130 °C further proves the association of P_3 with the α-form. P_3 was apparently merged with P_4 due to the increase in the thickness of corresponding lamella with annealing time and eventually transformed to that of the preexisting P_4 crystalline lamellae of more perfect α-form. Nevertheless, P_4 again merged with P_5 with subsequent increase in the β-form population as the annealing time was prolonged further.

Upon annealing of precrystallized PHT samples, the population of the β-form was found to increase signifi-

cantly at the expense of the α-form through melting/recrystallization, while the spherulitic morphology remained unchanged. Earlier studies have shown that both PTT and PPT exhibit ringed patterns in spherulites within a temperature window of crystallization. But PHT in this study exhibits no ring patterns, similar to PBT. Interestingly, the number of methylene groups between the terephthalate groups seems to determine the lamellar orientation leading to existence or absence of ring patterns within the spherulites. This is true for the homologous series of aryl polyesters, but may not be so for other types of polymers. Future work and studies seem urgent in order to fully expound this intriguing behavior.

Acknowledgment. The work has been supported by research grants in consecutive years from Taiwan National Science Council (#NSC 92-2216-E006-002, 93-2216-E006-024). Dr. A. K. Ghosh is financially sponsored by the Taiwan's National Science Council as a postdoctoral fellow for a term of one and a half years.

References and Notes

(1) Schmidtke, J.; Strobl, G.; Thurn-Albrecht, T. *Macromolecules* **1997**, *30*, 5804.
(2) De Rosa, C.; Auriemma, F.; Vinti, V.; Galimberti, M. *Macromolecules* **1998**, *31*, 6206.
(3) Woo, E. M.; Sun, Y. S.; Yang, C. P. *Prog. Polym. Sci.* **2001**, *26*, 945.
(4) Cheng, S. Z. D.; Cho, M. Y.; Wunderlich, B. *Macromolecules* **1986**, *19*, 1868.
(5) Medellín-Rodríguez, F. J.; Phillips, P. J.; Lin, J. S. *Macromolecules* **1996**, *29*, 7491.
(6) Chung, J. S.; Cebe, P. J. *J. Polym. Sci., Part B: Polym. Phys.* **1992**, *30*, 163.
(7) Woo, E. M.; Ko, T. Y. *Colloid Polym. Sci.* **1996**, *274*, 309.
(8) Wang, Z. G.; Hsiao, B. S.; Sauer, B. B.; Kampert, W. G. *Polymer* **1999**, *40*, 4615.
(9) Stein, R. S.; Misra, A. *J. Polym. Sci., Part B: Polym. Phys.* **1980**, *18*, 327.
(10) Yeh, J. Y.; Runt, J. *J. Polym. Sci., Part B: Polym. Phys.* **1989**, *27*, 1543.
(11) Runt, J.; Miley, D. M.; Zhang, X.; Gallagher, K. P.; McFeaters, K.; Fishburn, J. *Macromolecules* **1992**, *25*, 1929.
(12) Righetti, M. C. *Thermochim. Acta* **1999**, *330*, 131.
(13) Blundell, D. J.; Osborn, B. N. *Polymer* **1983**, *24*, 953.
(14) Blundell, D. J. *Polymer* **1987**, *28*, 2248.
(15) Hsiao, B. S.; Gardner, K. H.; Wu, D. Q. *Polymer* **1993**, *34*, 3996.
(16) Wu, P. L.; Woo, E. M. *J. Polym. Sci., Part B: Polym. Phys.* **2002**, *40*, 1571.
(17) Wu, P. L. Ph.D. Thesis, Department of Chemical Engineering, National Cheng Kung University, Tainan, Taiwan, 2003.
(18) Woo, E. M.; Wu, P. L.; Chiang, C. P.; Liu, H. L. *Macromol. Rapid Commun.* **2004**, *25*, 942.
(19) Yokouchi, M.; Sakakibara, Y.; Chatani, Y.; Tadokoro, H.; Tanaka, T.; Yoda, K. *Macromolecules* **1976**, *9*, 266.
(20) Hall, I. H.; Pass, M. G.; Rammo, N. N. *J. Polym. Sci., Part B: Polym. Phys.* **1978**, *16*, 1409.
(21) Hall, I. H.; Rammo, N. N. *J. Polym. Sci., Part B: Polym. Phys.* **1978**, *16*, 2189.
(22) Hall, I. H.; Ibrahim, B. A. *Polymer* **1982**, *23*, 805.
(23) Palmer, A.; Poulin-Dandurand, S.; Revol, J. F.; Brisse, F. *Eur. Polym. J.* **1984**, *20*, 783.
(24) Brisse, F.; Palmer, A.; Moss, B.; Dorset, D.; Roughead, A.; Miller, D. P. *Eur. Polym. J.* **1984**, *20*, 791.
(25) Lefèvre, C.; Villers, D.; Koch, M. H. J.; David, C. *Polymer* **2001**, *42*, 8769.
(26) Lee, J. H.; Jeong, Y. G.; Lee, S. C.; Min, B. G.; Jo, W. H. *Polymer* **2002**, *43*, 5263.
(27) David, C.; Lefèbvre, X.; Lefèvre, C.; Demarteau, W.; Loutz, J. M. *Prog. Org. Coat.* **1999**, *35*, 45.
(28) Lefèbvre, X.; Koch, M. H. J.; Reynaers, H.; David, C. *J. Polym. Sci., Part B: Polym. Phys.* **1999**, *37*, 1.
(29) Ghosh, A. K.; Woo, E. M. *J. Mater. Chem.* **2004**, *14*, 3034.
(30) Gilbert, M.; Hybart, F. J. *Polymer* **1972**, *13*, 327.
(31) Strobl, G. R.; Schneider, M. *J. Polym. Sci., Polym. Phys. Ed.* **1980**, *18*, 1343.
(32) Medellín-Rodríguez, F. J.; Phillips, P. J.; Lin, J. S. *Macromolecules* **1996**, *29*, 7491.
(33) Talibuddin, S.; Wu, L.; Runt, J.; Lin, J. S. *Macromolecules* **1996,** *29*, 7527.
(34) Chen, H. L.; Li, L. J.; Lin, T. L. *Macromolecules* **1998**, *31*, 2255.

MA0473667